# Efficient explicit solvers for multipatch discontinuous Galerkin isogeometric analysis

Jesse Chan[1], J. A. Evans[2]

[1]Department of Computational and Applied Math, Rice University
[2]Ann and H.J. Smead Aerospace Engineering Sciences, UC Boulder

ECCM-ECFD 2018
June 9-15, 2018

# High order methods for hyperbolic PDEs

- Time-dependent solutions of hyperbolic equations.
- Low numerical dissipation and dispersion.
- High order approximations: more accurate per unknown.
- High performance on many-core (explicit time-stepping).

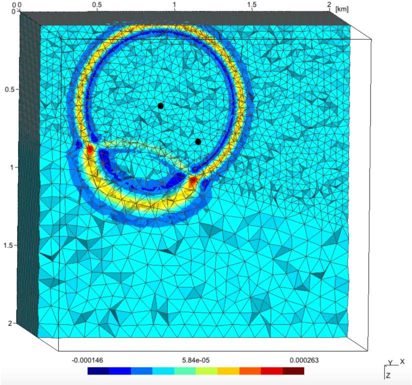


Figure courtesy of Axel Modave.

# High order methods for hyperbolic PDEs

- Time-dependent solutions of hyperbolic equations.
- Low numerical dissipation and dispersion.
- High order approximations: more accurate per unknown.
- High performance on many-core (explicit time-stepping).

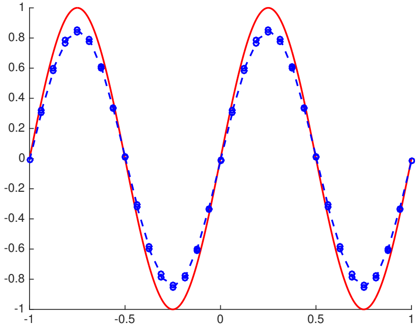


**Fine** linear approximation.

# High order methods for hyperbolic PDEs

- Time-dependent solutions of hyperbolic equations.
- Low numerical dissipation and dispersion.
- High order approximations: more accurate per unknown.
- High performance on many-core (explicit time-stepping).

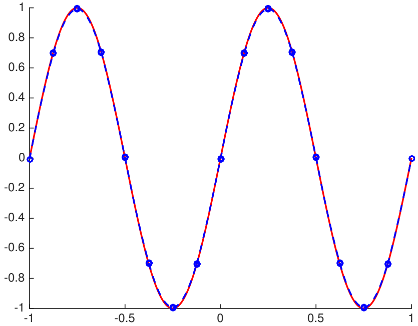


**Coarse** quadratic approximation.

# High order methods for hyperbolic PDEs

- Time-dependent solutions of hyperbolic equations.
- Low numerical dissipation and dispersion.
- High order approximations: more accurate per unknown.
- High performance on many-core (explicit time-stepping).

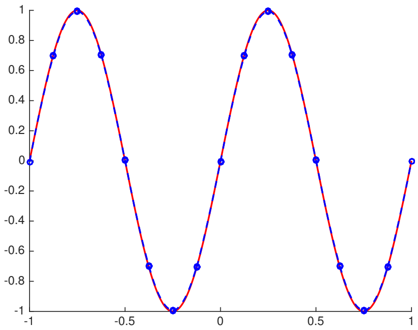


**Coarse** quadratic approximation.

# High order methods for hyperbolic PDEs

- Time-dependent solutions of hyperbolic equations.
- Low numerical dissipation and dispersion.
- High order approximations: more accurate per unknown.
- High performance on many-core (explicit time-stepping).

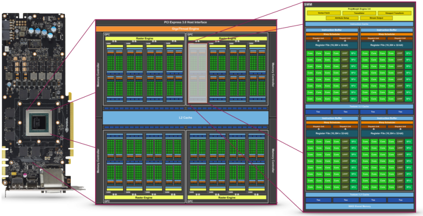

A graphics processing unit (GPU).

# Multi-patch discontinuous Galerkin formulations

- Wave propagation problems (acoustics, Maxwells, elasticity).
- Model problem: acoustic wave equation (both first and second order formulations)

$$\frac{1}{c^2}\frac{\partial p}{\partial t} + \nabla \cdot \boldsymbol{u} = f$$
$$\frac{\partial \boldsymbol{u}}{\partial t} + \nabla p = 0.$$

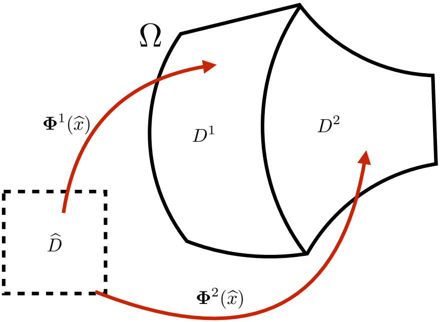


- Multiple geometric patches, weak patch coupling through DG-like numerical interface flux (SIPG, upwind).

Langer et al (2014). *Multipatch discontinuous Galerkin isogeometric analysis*.

Wilcox et al (2010). *A high-order DG method for wave propagation through coupled elastic-acoustic media*.

# Explicit solvers for multi-patch DG-IGA

- Semi-discrete system:

$$\boldsymbol{M}_h \frac{\mathrm{d}\boldsymbol{u}}{\mathrm{d}t} = \boldsymbol{A}_h \boldsymbol{u} \quad \Rightarrow \quad \frac{\mathrm{d}\boldsymbol{u}}{\mathrm{d}t} = \boldsymbol{M}_h^{-1} \boldsymbol{A}_h \boldsymbol{u}.$$

- Global mass matrix $\boldsymbol{M}_h$ is (patch) block diagonal.
- Challenges and questions:
  - How to efficiently invert 3D patch mass matrices while guaranteeing accuracy and stability (especially for explicit methods)?
  - Do splines/IGA offer advantages over $C^0$-FEM/DG for explicit solvers?
  - Can we tailor IGA discretizations towards explicit time-stepping?

# Explicit solvers for multi-patch DG-IGA

- Semi-discrete system:

$$\boldsymbol{M}_h \frac{\mathrm{d}\boldsymbol{u}}{\mathrm{d}t} = \boldsymbol{A}_h \boldsymbol{u} \quad \Rightarrow \quad \frac{\mathrm{d}\boldsymbol{u}}{\mathrm{d}t} = \boldsymbol{M}_h^{-1} \boldsymbol{A}_h \boldsymbol{u}.$$

- Global mass matrix $\boldsymbol{M}_h$ is (patch) block diagonal.

- Challenges and questions:
  - How to efficiently invert 3D patch mass matrices while guaranteeing accuracy and stability (especially for explicit methods)?
  - Do splines/IGA offer advantages over $C^0$-FEM/DG for explicit solvers?
  - Can we tailor IGA discretizations towards explicit time-stepping?

# Explicit solvers for multi-patch DG-IGA

- Semi-discrete system:

$$\boldsymbol{M}_h \frac{\mathrm{d}\boldsymbol{u}}{\mathrm{d}t} = \boldsymbol{A}_h \boldsymbol{u} \quad \Rightarrow \quad \frac{\mathrm{d}\boldsymbol{u}}{\mathrm{d}t} = \boldsymbol{M}_h^{-1} \boldsymbol{A}_h \boldsymbol{u}.$$

- Global mass matrix $\boldsymbol{M}_h$ is (patch) block diagonal.
- Challenges and questions:
  - How to efficiently invert 3D patch mass matrices while guaranteeing accuracy and stability (especially for explicit methods)?
  - Do splines/IGA offer advantages over $C^0$-FEM/DG for explicit solvers?
  - Can we tailor IGA discretizations towards explicit time-stepping?

# Explicit solvers for multi-patch DG-IGA

- Semi-discrete system:

$$\boldsymbol{M}_h \frac{\mathrm{d}\boldsymbol{u}}{\mathrm{d}t} = \boldsymbol{A}_h \boldsymbol{u} \quad \Rightarrow \quad \frac{\mathrm{d}\boldsymbol{u}}{\mathrm{d}t} = \boldsymbol{M}_h^{-1} \boldsymbol{A}_h \boldsymbol{u}.$$

- Global mass matrix $\boldsymbol{M}_h$ is (patch) block diagonal.

- Challenges and questions:
  - How to efficiently invert 3D patch mass matrices while guaranteeing accuracy and stability (especially for explicit methods)?
  - Do splines/IGA offer advantages over $C^0$-FEM/DG for explicit solvers?
  - Can we tailor IGA discretizations towards explicit time-stepping?

# Outline

# Outline

# B-splines: assumptions for this talk

- Reference coordinates $\widehat{\boldsymbol{x}} \in \widehat{D}$, physical coordinates $\boldsymbol{x} \in D^k$.
- Standard 1D B-splines: $B_i^0(\widehat{x}) = \mathbb{1}_{\xi_i \leq \widehat{x} \leq \xi_{i+1}}$,

$$B_i^k(\widehat{x}) = \frac{\widehat{x} - \xi_i}{\xi_{i+p} - \xi_i} B_i^{k-1}(\widehat{x}) + \frac{\xi_{i+p+1} - \widehat{x}}{\xi_{i+p+1} - \xi_{i+1}} B_{i+1}^{k-1}(\widehat{x}).$$

- Physical basis: mapping of tensor product basis on reference domain

$$B_{ijk}^p(\widehat{\boldsymbol{x}}) = B_i^p(\widehat{x}) B_j^p(\widehat{y}) B_k^p(\widehat{z}).$$

- Assume maximally continuous, open knot vectors

$$\xi_{p+1} < \ldots < \xi_{p+1+K},$$
$$\xi_1 = \ldots = \xi_{p+1},$$
$$\xi_{p+1+K} = \ldots = \xi_{2p+1+K}.$$

# IGA mass matrices: stability/accuracy vs efficiency

- Energy stability: if $\boldsymbol{u}^T \boldsymbol{A}_h \boldsymbol{u} \leq 0$, semi-discrete solution won't blow up

$$\boldsymbol{M}_h \frac{\mathrm{d}\boldsymbol{u}}{\mathrm{d}t} = \boldsymbol{A}_h \boldsymbol{u} \quad \Longrightarrow \quad \frac{\mathrm{d}}{\mathrm{d}t}\left(\boldsymbol{u}^T \boldsymbol{M}_h \boldsymbol{u}\right) = \frac{1}{2}\frac{\partial}{\partial t}\|u\|_{L^2}^2 \leq 0.$$

- Approximating $\boldsymbol{M}_h^{-1}$ impacts semi-discrete stability and accuracy.

- Curved patch mass matrices $\boldsymbol{M}_J$: tensor product basis $B^p_{ijk}(\widehat{\boldsymbol{x}})$

$$\left(\boldsymbol{M}_J\right)_{ijk,lmn} = \int_{\widehat{D}} B^p_{ijk}(\widehat{\boldsymbol{x}}) B^p_{lmn}(\widehat{\boldsymbol{x}}) J(\widehat{\boldsymbol{x}})\, \mathrm{d}\widehat{\boldsymbol{x}}, \qquad \text{(B-splines)}$$

- No Kronecker structure due to $J(\widehat{\boldsymbol{x}})$: $\boldsymbol{M}_h$ expensive to invert in 3D!

# IGA mass matrices: stability/accuracy vs efficiency

- Energy stability: if $\boldsymbol{u}^T \boldsymbol{A}_h \boldsymbol{u} \leq 0$, semi-discrete solution won't blow up

$$\boldsymbol{M}_h \frac{\mathrm{d}\boldsymbol{u}}{\mathrm{d}t} = \boldsymbol{A}_h \boldsymbol{u} \quad \Longrightarrow \quad \frac{\mathrm{d}}{\mathrm{d}t}\left(\boldsymbol{u}^T \boldsymbol{M}_h \boldsymbol{u}\right) = \frac{1}{2}\frac{\partial}{\partial t}\|u\|_{L^2}^2 \leq 0.$$

- Approximating $\boldsymbol{M}_h^{-1}$ impacts semi-discrete stability and accuracy.

- Curved patch mass matrices $\boldsymbol{M}_J$: tensor product basis $B^p_{ijk}(\widehat{\boldsymbol{x}})$

$$(\boldsymbol{M}_J)_{ijk,lmn} = \int_{\widehat{D}} B^p_{ijk}(\widehat{\boldsymbol{x}}) B^p_{lmn}(\widehat{\boldsymbol{x}}) J(\widehat{\boldsymbol{x}}) \,\mathrm{d}\widehat{\boldsymbol{x}}, \qquad \text{(B-splines)}$$

- No Kronecker structure due to $J(\widehat{\boldsymbol{x}})$: $\boldsymbol{M}_h$ expensive to invert in 3D!

# IGA mass matrices: stability/accuracy vs efficiency

- Energy stability: if $\boldsymbol{u}^T \boldsymbol{A}_h \boldsymbol{u} \leq 0$, semi-discrete solution won't blow up

$$\boldsymbol{M}_h \frac{\mathrm{d}\boldsymbol{u}}{\mathrm{d}t} = \boldsymbol{A}_h \boldsymbol{u} \quad \Longrightarrow \quad \frac{\mathrm{d}}{\mathrm{d}t}\left(\boldsymbol{u}^T \boldsymbol{M}_h \boldsymbol{u}\right) = \frac{1}{2}\frac{\partial}{\partial t}\|u\|_{L^2}^2 \leq 0.$$

- Approximating $\boldsymbol{M}_h^{-1}$ impacts semi-discrete stability and accuracy.

- Curved patch mass matrices $\boldsymbol{M}_J$: tensor product basis $B_{ijk}^p(\widehat{\boldsymbol{x}})$

$$(\boldsymbol{M}_J)_{ijk,lmn} = \int_{\widehat{D}} \frac{B_{ijk}^p(\widehat{\boldsymbol{x}})}{w_R(\widehat{\boldsymbol{x}})} \frac{B_{lmn}^p(\widehat{\boldsymbol{x}})}{w_R(\widehat{\boldsymbol{x}})} J(\widehat{\boldsymbol{x}})\, \mathrm{d}\widehat{\boldsymbol{x}} \qquad \text{(NURBS)}$$

- No Kronecker structure due to $J(\widehat{\boldsymbol{x}})$: $\boldsymbol{M}_h$ expensive to invert in 3D!

# IGA mass matrices: stability/accuracy vs efficiency

- Energy stability: if $\boldsymbol{u}^T \boldsymbol{A}_h \boldsymbol{u} \leq 0$, semi-discrete solution won't blow up

$$\boldsymbol{M}_h \frac{\mathrm{d}\boldsymbol{u}}{\mathrm{d}t} = \boldsymbol{A}_h \boldsymbol{u} \quad \Longrightarrow \quad \frac{\mathrm{d}}{\mathrm{d}t}\left(\boldsymbol{u}^T \boldsymbol{M}_h \boldsymbol{u}\right) = \frac{1}{2}\frac{\partial}{\partial t}\|u\|_{L^2}^2 \leq 0.$$

- Approximating $\boldsymbol{M}_h^{-1}$ impacts semi-discrete stability and accuracy.

- Curved patch mass matrices $\boldsymbol{M}_J$: tensor product basis $B_{ijk}^p(\widehat{\boldsymbol{x}})$

$$(\boldsymbol{M}_J)_{ijk,lmn} = \int_{\widehat{D}} B_{ijk}^p(\widehat{\boldsymbol{x}}) B_{lmn}^p(\widehat{\boldsymbol{x}}) \frac{J(\widehat{\boldsymbol{x}})}{w_R^2(\widehat{\boldsymbol{x}})} \, \mathrm{d}\widehat{\boldsymbol{x}} \qquad \text{(NURBS)}$$

- No Kronecker structure due to $J(\widehat{\boldsymbol{x}})$: $\boldsymbol{M}_h$ expensive to invert in 3D!

# Approximate mass matrix inversion

- Mass lumping: loss of high order accuracy for IGA.
- Preconditioning:
  - Additional cost and complexity for a time-domain code.
  - Semi-discrete stability requires approximation of $\boldsymbol{M}_J^{-1}$ to induce a norm on $\boldsymbol{u}$ (e.g. a fixed symmetric positive-definite linear operator).
  - Example: Krylov methods approximate $\boldsymbol{M}_J^{-1}$ as a non-linear operator!
- Isogeometric collocation: restores tensor product structure, but semi-discrete stability is more difficult to prove.

---

Gao and Calo (2014). *Fast isogeometric solvers for explicit dynamics*.

Evans, Hiemstra, Hughes, Reali (2017). *Explicit higher-order accurate IG collocation methods for structural dynamics*.

Wathen and Rees (2009). *Chebyshev semi-iteration in preconditioning for problems including the mass matrix*.

Auricchio et al (2012). *Isogeometric collocation for elastostatics and explicit dynamics*.

# An energy stable and efficient approximation to $\boldsymbol{M}^{-1}$

- Replace $\boldsymbol{M}_J$ with symmetric pos-def "weight-adjusted" approximation:

$$\boldsymbol{M}_J \boldsymbol{u} \Rightarrow \widehat{\boldsymbol{M}} \boldsymbol{M}_{1/J}^{-1} \widehat{\boldsymbol{M}} \boldsymbol{u}, \qquad \left(\widehat{\boldsymbol{M}}\right)_{ijk,lmn} = \int_{\widehat{D}} B^p_{ijk}(\widehat{\boldsymbol{x}}) B^p_{lmn}(\widehat{\boldsymbol{x}}) \,\mathrm{d}\widehat{\boldsymbol{x}}.$$

- Weight-adjusted inverse: Kronecker product, matrix-free eval. of $\boldsymbol{M}_{1/J}$

$$\boldsymbol{M}_J^{-1} \approx \left(\widehat{\boldsymbol{M}} \boldsymbol{M}_{1/J}^{-1} \widehat{\boldsymbol{M}}\right)^{-1} = \widehat{\boldsymbol{M}}^{-1} \boldsymbol{M}_{1/J} \widehat{\boldsymbol{M}}^{-1}$$
$$\widehat{\boldsymbol{M}}^{-1} = \widehat{\boldsymbol{M}}_{\mathrm{1D}}^{-1} \otimes \widehat{\boldsymbol{M}}_{\mathrm{1D}}^{-1} \otimes \widehat{\boldsymbol{M}}_{\mathrm{1D}}^{-1}.$$

- Energy stability with respect to an equivalent norm

$$C_1(J) \left\|\boldsymbol{u}\right\|_{\widehat{\boldsymbol{M}} \boldsymbol{M}_{1/J}^{-1} \widehat{\boldsymbol{M}}} \leq \left\|\boldsymbol{u}\right\|_{\boldsymbol{M}_J} \leq C_2 \left\|\boldsymbol{u}\right\|_{\widehat{\boldsymbol{M}} \boldsymbol{M}_{1/J}^{-1} \widehat{\boldsymbol{M}}}.$$

---

Chan, Hewett, Warburton (2016). *Weight-adjusted DG methods: wave prop. in heterogeneous media.*

Chan, Hewett, Warburton (2016). *Weight-adjusted DG methods: curvilinear meshes.*

# Accuracy: weighted vs weight-adjusted mass matrix

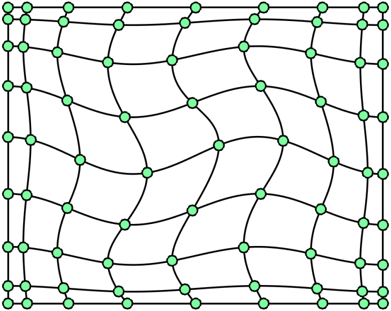

(a) Warped mesh

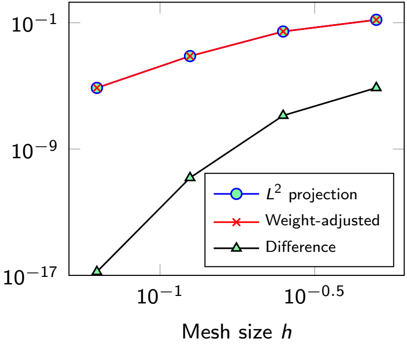


(b) Error for acoustics (first order form)

Figure: $L^2$ errors for the acoustic wave equation using weighted and weight-adjusted mass matrices for tensor product $p = 4$ splines.

# Accuracy: weighted vs weight-adjusted mass matrix

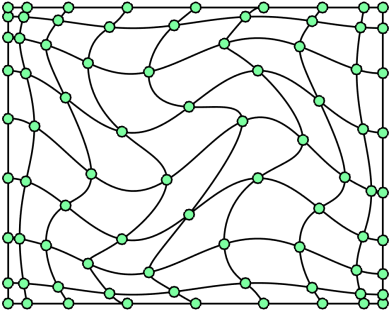

(a) Warped mesh

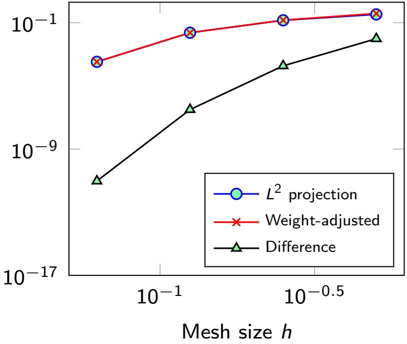


(b) Error for acoustics (first order form)

Figure: $L^2$ errors for the acoustic wave equation using weighted and weight-adjusted mass matrices for tensor product $p = 4$ splines.

# Accuracy of the weight-adjusted mass matrix

- Difference between the weighted $L^2$ and weight-adjusted inner products is high order accurate: for $v(\boldsymbol{x})$ of degree $q$,

$$\left|\boldsymbol{v}^T \boldsymbol{M}_J \boldsymbol{u} - \boldsymbol{v}^T \widehat{\boldsymbol{M}} \boldsymbol{M}_{1/J}^{-1} \widehat{\boldsymbol{M}} \boldsymbol{u}\right| \\ \leq C_J \left\|J\right\|_{W^{p+1,\infty}\left(D^k\right)} h^{2p+2-q} \left\|u\right\|_{W^{p+1,2}\left(D^k\right)}.$$

- Difference between $L^2$ and weight-adjusted projection is $O(h^{p+2})$!

$$\left\|P_h u - \tilde{P}_h u\right\|_{L^2\left(D^k\right)} \lesssim \left\|\frac{1}{\sqrt{J}}\right\|_{L^\infty}^2 \left\|J\right\|_{W^{p+1,\infty}\left(D^k\right)} h^{p+2} \left\|u\right\|_{W^{p+1,2}\left(D^k\right)}.$$

Chan, Wilcox (2018). *On discretely entropy stable weight-adjusted discontinuous Galerkin methods: curvilinear meshes.*

# Estimating the CFL restriction

- For explicit time-stepping method: estimate $dt \propto \frac{1}{\max|\lambda_j|}$

$$\boldsymbol{M}_h \boldsymbol{v} = \lambda \boldsymbol{A}_h \boldsymbol{v}.$$

- Bendixon-Hirsch lemma: bound $\mathrm{Re}\left(\lambda_j\right), \mathrm{Im}\left(\lambda_j\right)$ using the symmetric and skew-symmetric parts of $\boldsymbol{A}_h$

$$\underbrace{\frac{1}{2}\left(\boldsymbol{A}_h + \boldsymbol{A}_h^T\right)}_{\boldsymbol{A}_{\mathrm{sym}}} + \underbrace{\frac{1}{2}\left(\boldsymbol{A}_h - \boldsymbol{A}_h^T\right)}_{\boldsymbol{A}_{\mathrm{skew}}}, \qquad \begin{aligned} \left|\mathrm{Re}\left(\lambda_j\right)\right| &\leq \rho\left(\boldsymbol{M}_h^{-1}\boldsymbol{A}_{\mathrm{sym}}\right), \\ \left|\mathrm{Im}\left(\lambda_j\right)\right| &\leq \rho\left(\boldsymbol{M}_h^{-1}\boldsymbol{A}_{\mathrm{skew}}\right). \end{aligned}$$

- $\rho\left(\boldsymbol{M}_h^{-1}\boldsymbol{A}_{\mathrm{sym}}\right), \rho\left(\boldsymbol{M}_h^{-1}\boldsymbol{A}_{\mathrm{skew}}\right)$: generalized Rayleigh quotients

$$\rho\left(\boldsymbol{M}_h^{-1}\boldsymbol{A}_{\mathrm{sym}}\right) = \frac{\boldsymbol{u}^T\boldsymbol{A}_{\mathrm{sym}}\boldsymbol{u}}{\boldsymbol{u}^T\boldsymbol{M}_h\boldsymbol{u}}, \qquad \rho\left(\boldsymbol{M}_h^{-1}\boldsymbol{A}_{\mathrm{skew}}\right) = \frac{\left|\boldsymbol{u}^*(i\boldsymbol{A}_{\mathrm{skew}})\boldsymbol{u}\right|}{\boldsymbol{u}^*\boldsymbol{M}_h\boldsymbol{u}}$$

# CFL: constants in trace and inverse inequalities

- For hyperbolic problems (advection, acoustics), can bound

$$\frac{\boldsymbol{u}^T \boldsymbol{A}_{\rm sym} \boldsymbol{u}}{\boldsymbol{u}^T \boldsymbol{M}_h \boldsymbol{u}} \lesssim \frac{\left\|u\right\|^2_{L^2(\partial D^k)}}{\left\|u\right\|^2_{L^2(D^k)}} \lesssim \frac{C_T}{h},$$

$$\frac{\left|\boldsymbol{u}^*(i\boldsymbol{A}_{\rm skew})\boldsymbol{u}\right|}{\boldsymbol{u}^* \boldsymbol{M}_h \boldsymbol{u}} \lesssim \frac{\left\|\nabla u\right\|_{L^2(D^k)}}{\left\|u\right\|_{L^2(D^k)}} \lesssim \frac{C_I}{h}.$$

- $C_T, C_I$: $p$-dependent constants in trace, inverse inequalities

$$\left\|\nabla u\right\|_{L^2(\widehat{D})} \leq C_I \left\|u\right\|_{L^2(\widehat{D})}, \qquad \left\|u\right\|^2_{L^2(\partial\widehat{D})} \leq C_T \left\|u\right\|^2_{L^2(\widehat{D})}.$$

- Summary: $dt \propto \frac{1}{\max|\lambda_j|} \leq \frac{h}{\max C_T, C_I}$. What do $C_T, C_I$ look like? Can compute $C_T, C_I$ using a generalized eigenvalue problem.

# Trace and inverse inequality constants: $C^0$-FEM vs splines

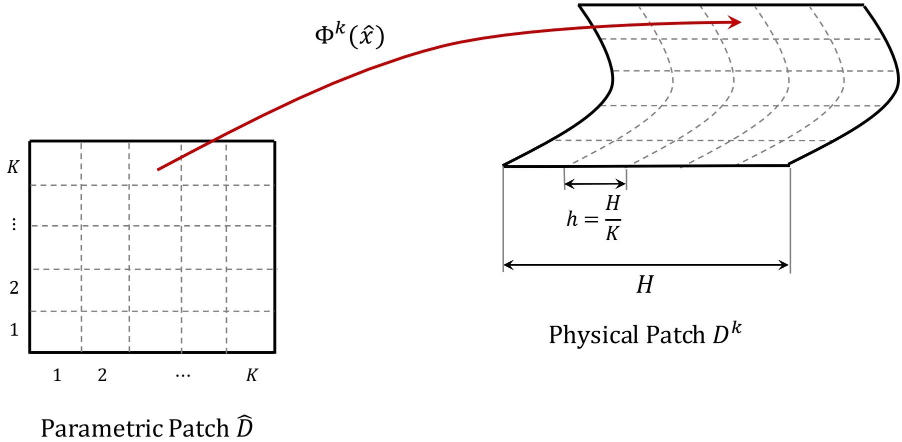


Figure: A parametric patch has $K$ elements per side, while a physical patch has size $H$. The mesh resolution is $h = H/K$.

# Trace and inverse inequality constants: $C^0$-FEM vs splines

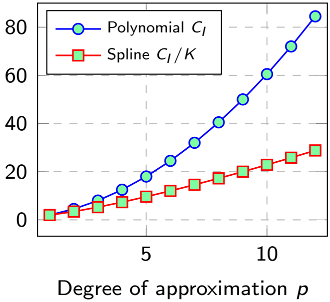


(a) Inverse constants, $K = 2p$

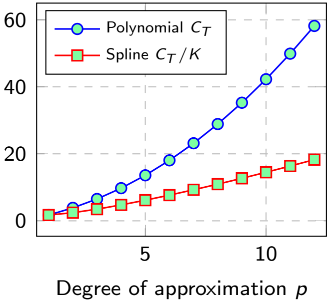


(b) Trace constants, $K = 2p$

Polynomial constants are $O(p^2)$, observed spline constants $O(p)$ for $K \geq O(1/p)$.

$dt \propto \frac{h}{p^2}$ for $C^0$-FEM and DG, $dt \propto \frac{h}{p}$ for IGA!

---

Takacs, Takacs (2016). *Approximation error estimates and inverse inequalities for B-splines of maximum smoothness.*

# Trace and inverse inequality constants: $C^0$-FEM vs splines

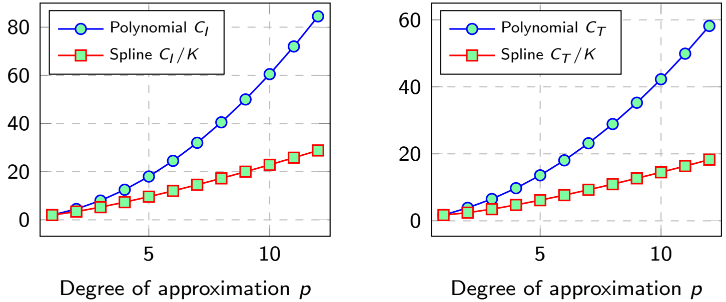


(a) Inverse constants, $K = 2p$

(b) Trace constants, $K = 2p$

Polynomial constants are $O(p^2)$, observed spline constants $O(p)$ for $K \geq O(1/p)$.

$$\boxed{dt \propto \frac{h}{p^2} \text{ for } C^0\text{-FEM and DG, } dt \propto \frac{h}{p} \text{ for IGA!}}$$

Takacs, Takacs (2016). *Approximation error estimates and inverse inequalities for B-splines of maximum smoothness.*

# B-spline bases and optimal spline spaces

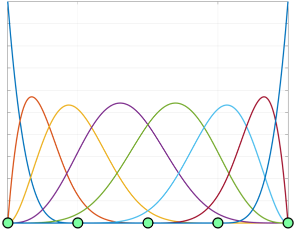

(c) Uniform knots

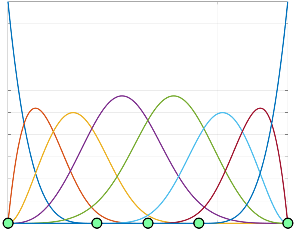

(d) Optimal knots

- Sup-inf: "worst best approximation" in $X$ from $X_n$

$$d_n(X; X_n) = \sup_{x \in X} \inf_{y \in X_n} \|x - y\|, \qquad \dim(X_n) = n.$$

- Spline spaces with optimal knot vectors: minimal sup-inf for

$$X = \left\{ f \in L^2([-1,1]) : \frac{\partial^{p-1} f}{\partial x^{p-1}} \text{ continuous}, \quad \|f\|_{L^2} \leq 1 \right\},$$

Melkman and Micchelli (1978). *Spline spaces are optimal for $L^2$ n-width.*

# Optimal knot vectors: roots of eigenfunctions

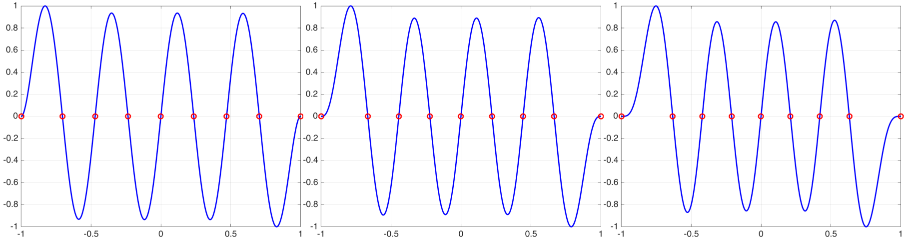


(a) $p = 2$ (b) $p = 3$ (c) $p = 4$

Figure: Eigenfunctions $y_{K+1,p}(x)$ for $K = 8$ and various $p$.

- Optimal knots are roots of eigenfunctions $y_{K+1,p}(x)$.

$$(-1)^p \frac{\partial^{2p} y}{\partial x^{2p}} = \lambda y(x), \qquad \frac{\partial^k y}{\partial x^k}(-1) = \frac{\partial^k y}{\partial x^k}(1) = 0, \quad 1 \leq k \leq p-1.$$

- Approximate $y_{K+1,p}(x)$ using fine spline space; difficult for high $K, p$!

# Knot smoothing: approximating optimal knots

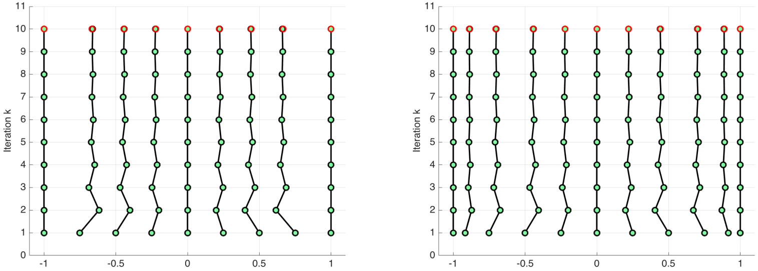


(a) Knots $\xi_i$ (optimal in red) (b) Greville abscissae $\tau_j$

- Greville abscissae $\tau_j$: coefficients for linear coordinate $x$.

$$x = \sum_{1 \leq j \leq p+K} \tau_j B_j^p(x), \qquad \tau_j = \frac{1}{p} \sum_{1 \leq i \leq p} \xi_{i+j-1}, \quad j = 1, \ldots, p.$$

- Replace Greville abscissae with equispaced points $\widehat{x}_i$ and iterate

$$\tilde{\xi}_i^{k+1} = \sum_{1 \leq j \leq p+K} \widehat{x}_i B_j^p(\xi_i; \tilde{\xi}^k), \qquad \tilde{\xi}_i^0 = \xi_i,$$

# Knot smoothing: approximating optimal knots

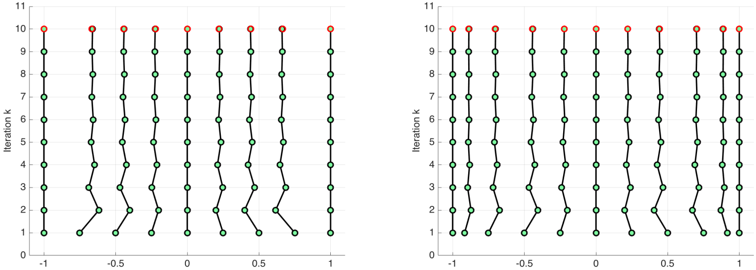


(a) Knots $\xi_i$ (optimal in red)

(b) Greville abscissae $\tau_j$

- Greville abscissae $\tau_j$: coefficients for linear coordinate $x$.

$$\color{red}{\xi_i} = \sum_{1 \leq j \leq p+K} \tau_j B_j^p(\color{red}{\xi_i}), \qquad \tau_j = \frac{1}{p} \sum_{1 \leq i \leq p} \xi_{i+j-1}, \quad j = 1, \ldots, p.$$

- Replace Greville abscissae with equispaced points $\widehat{x}_i$ and iterate

$$\tilde{\xi}_i^{k+1} = \sum_{1 \leq j \leq p+K} \widehat{x}_i B_j^p(\xi_i; \tilde{\xi}^k), \qquad \tilde{\xi}_i^0 = \xi_i,$$

# Approximation properties in 1D: oscillatory functions

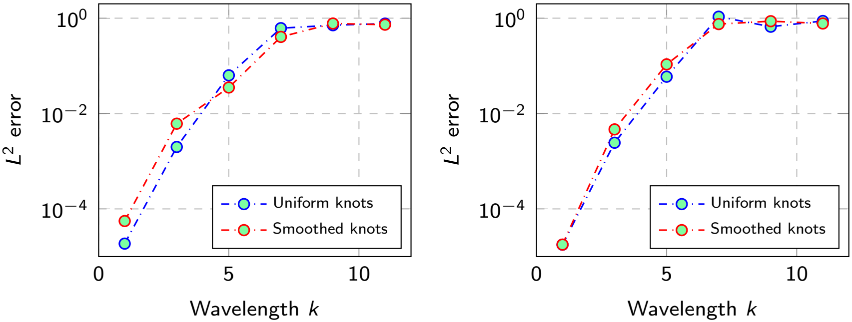


(a) First order formulation

(b) Second order formulation

Figure: $L^2$ errors for 1D acoustics using uniform and smoothed knot vectors: smoothed knots emphasize high frequencies over low frequencies.

# Approximation properties in 2D/3D: curvilinear domains

- Smoothed knot vectors: more accurate on curved domains.
- Differences between first, second order forms ($L^2$ vs energy norm?).

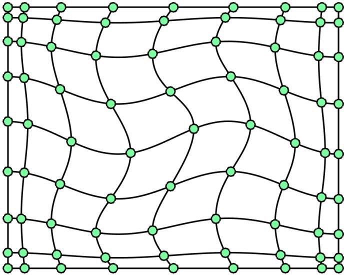

(a) Warped mesh, $\alpha = 1/8$

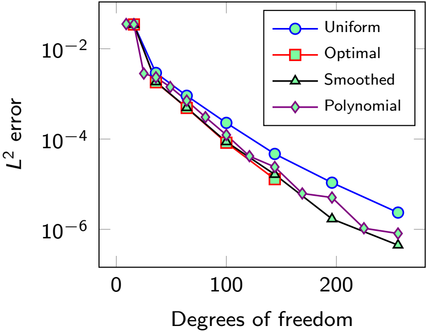


(b) $L^2$ errors ($\alpha = 1/64$)

Figure: $L^2$ approx. errors: $\cos\left(\frac{\pi x}{2}\right)\cos\left(\frac{\pi y}{2}\right)$, $p = 2, \ldots, 8$ and $K = p$.

# Approximation properties in 2D/3D: curvilinear domains

- Smoothed knot vectors: more accurate on curved domains.
- Differences between first, second order forms ($L^2$ vs energy norm?).

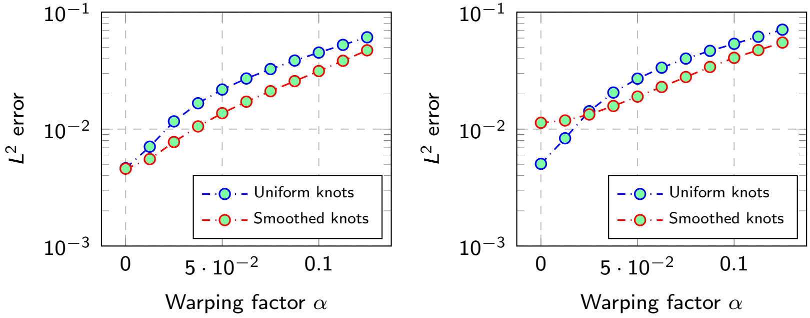


(a) First order formulation (b) Second order formulation

Figure: $L^2$ errors w.r.t. curved warping for 2D acoustics ($p = 3, K = 8$ splines).

# Smoothed knot vectors improve the CFL

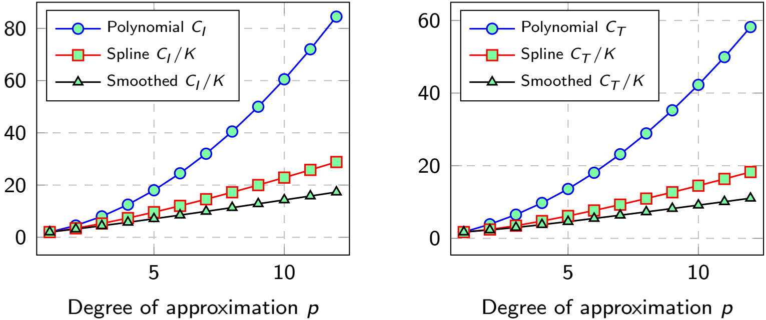


(a) Inverse constants, $K = 2p$ (b) Trace constants, $K = 2p$

Figure: Knot smoothing results in roughly $2\times$ smaller trace, inverse constants.

# Smoothed knot vectors improve the CFL

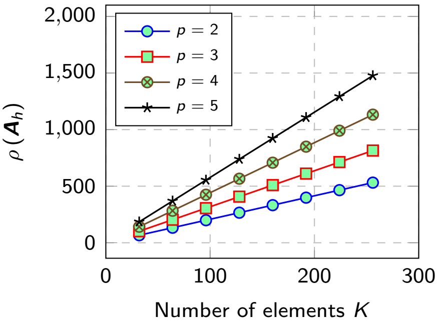


(a) Uniform knots

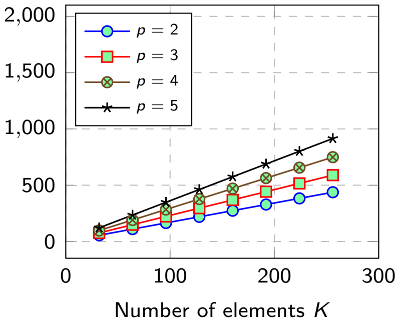


(b) Smoothed knots

Figure: Growth of $\rho(\boldsymbol{A}_h)$ for advection using spline spaces of degree $p = 2, \ldots, 5$.

# Smoothed knot vectors improve the CFL

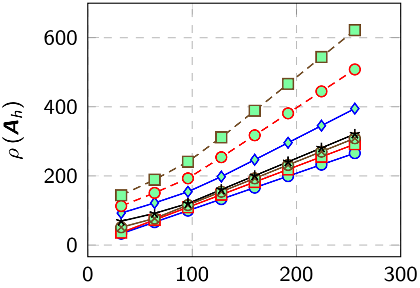


(a) Uniform knots

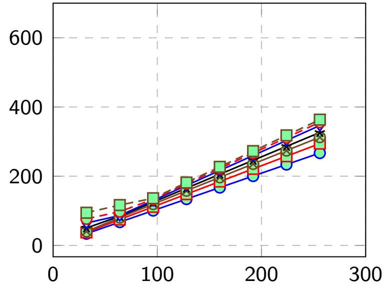


(b) Smoothed knots

Figure: Growth of $\rho(\boldsymbol{A}_h)$ using an upwind flux and spline spaces of degree $p = 2, \ldots, 8$. Nearly $p$-independent CFL observed for advection, acoustics.

# Acoustics: a 3D multi-patch example

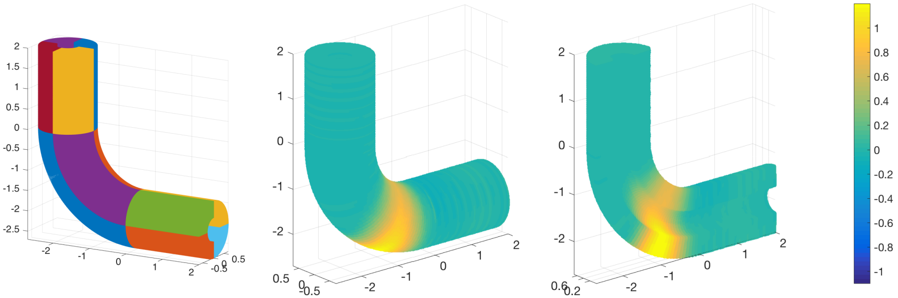

- 12 patch pipe model, first order formulation, pulse inflow condition.
- Isotropic $p = 6, K = 16$ splines, smoothed knots on each patch.

# Summary and acknowledgements

- Weight-adjusted mass matrix: restore Kronecker structure while retaining energy stability and high order accuracy.
- Improved $O(h/p)$ CFL scaling for IGA, optimal $L^2$ convergence rates.
- Smoothed knots: improved CFL, better curved approximations.
- Future directions: curl-conforming spline spaces (Maxwells).
- This research is supported by DMS-1719818 and DMS-1712639.

Thank you! Questions?

Chan, Evans (2018). *Multi-patch discontinuous Galerkin isogeometric analysis for wave propagation: explicit time-stepping and efficient mass matrix inversion.*

# Additional slides

# Patch refinement vs knot insertion (uniform knots)

- Patch size $H$, number of sub-elements $K$: $h = H/K$.
- Optimal $O(h^{p+1})$ $L^2$ error for both patch refinement, knot insertion.

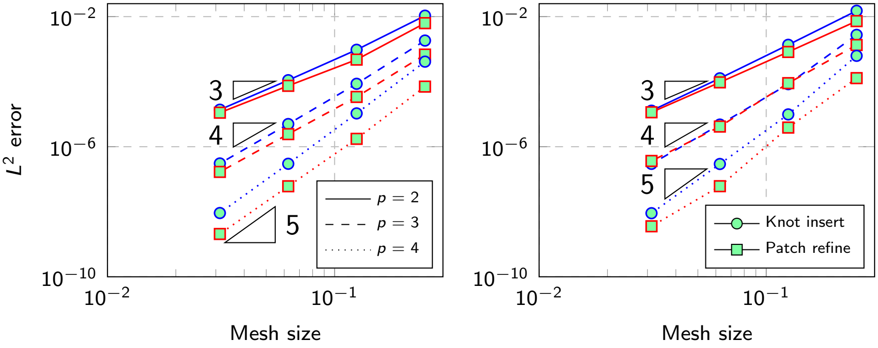


(a) First order (uniform knots) (b) Second order (uniform knots)

# Behavior of weight-adjusted $L^2$ projection

Comparison with $L^2$ projection and Low-Storage Curvilinear DG

$$\tilde{\phi}_i = \frac{\phi_i}{\sqrt{J}}, \qquad \boldsymbol{M}_{ij} = \int_{D^k} \tilde{\phi}_j \tilde{\phi}_i J = \int_{\widehat{D}} \phi_j \phi_i = \widehat{\boldsymbol{M}}_{ij}.$$

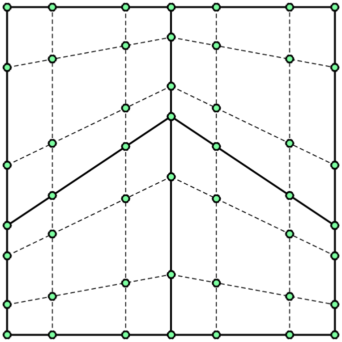

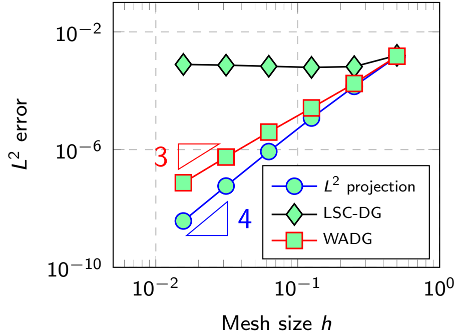


Figure: Arnold-type mesh with $\|J\|_{W^{N+1,\infty}} = O(h^{-1})$ for $N = 3$.

# Behavior of weight-adjusted $L^2$ projection

Comparison with $L^2$ projection and Low-Storage Curvilinear DG

$$\tilde{\phi}_i = \frac{\phi_i}{\sqrt{J}}, \qquad \boldsymbol{M}_{ij} = \int_{D^k} \tilde{\phi}_j \tilde{\phi}_i J = \int_{\widehat{D}} \phi_j \phi_i = \widehat{\boldsymbol{M}}_{ij}.$$

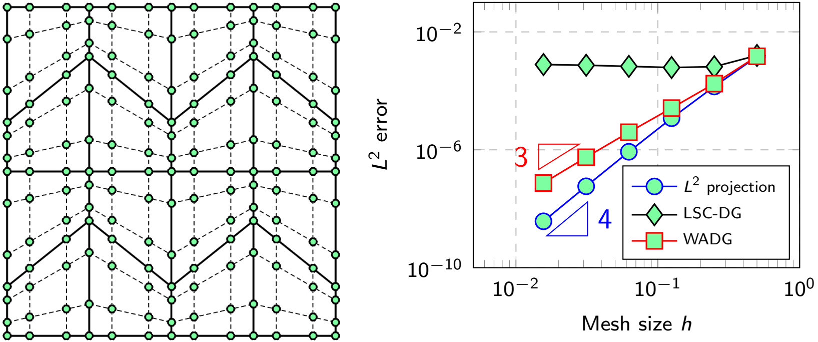


Figure: Arnold-type mesh with $\|J\|_{W^{N+1,\infty}} = O(h^{-1})$ for $N = 3$.

# Behavior of weight-adjusted $L^2$ projection

Comparison with $L^2$ projection and Low-Storage Curvilinear DG

$$\tilde{\phi}_i = \frac{\phi_i}{\sqrt{J}}, \qquad \boldsymbol{M}_{ij} = \int_{D^k} \tilde{\phi}_j \tilde{\phi}_i J = \int_{\widehat{D}} \phi_j \phi_i = \widehat{\boldsymbol{M}}_{ij}.$$

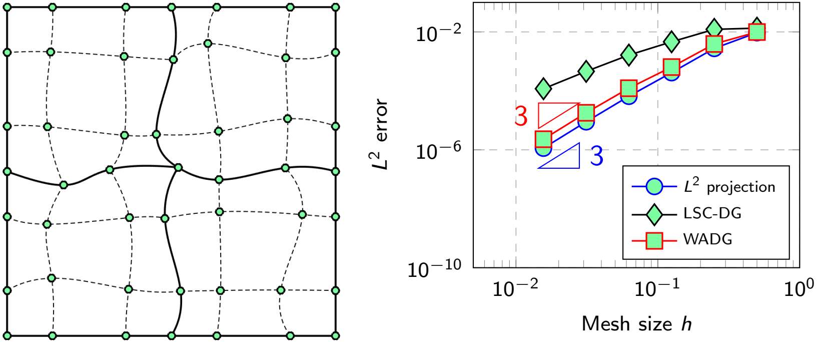


Figure: Curvilinear mesh constructed through random perturbation for $N = 3$.

# Behavior of weight-adjusted $L^2$ projection

High order convergence slowed by growth of $\|J\|_{W^{N+1,\infty}} = O(h^N)$.

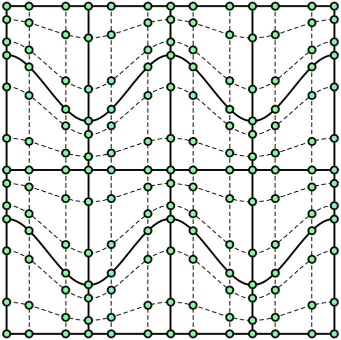

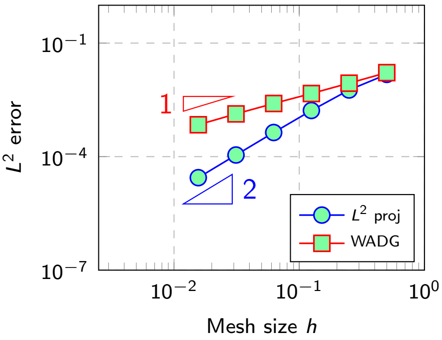


Figure: Moderately warped curved Arnold-type mesh for $N = 3$.

# Behavior of weight-adjusted $L^2$ projection

High order convergence is stalled by growth of $\|J\|_{W^{N+1,\infty}} = O(h^{N+1})$.

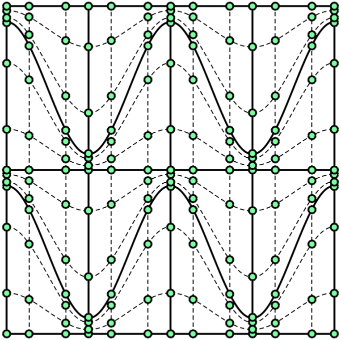

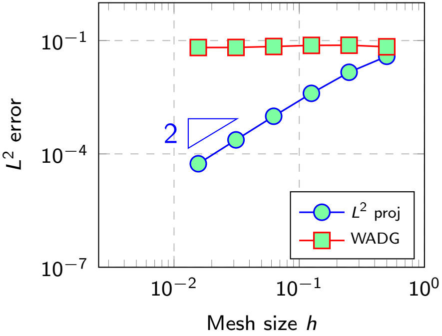


Figure: Heavily warped curved Arnold-type mesh for $N = 3$.

# Weight-adjusted DG: not locally conservative

- Con: loss of local conservation for $w(x) \notin P^N$!
- Pro: superconvergence of conservation error

$$\text{Conservation error} \leq C h^{2N+2} \|w\|_{W^{N+1,\infty}} \|p\|_{W^{N+1,2}}$$

where $C$ depends on mesh quality and max/min values of $w$.

- Pro: can restore local conservation with rank-1 update (Shermann-Morrison).

# Effect of conservation on shock speeds

- Weighted Burgers' equation, $w(x)$ curves characteristic lines.

$$w(x)\frac{\partial u}{\partial t} + \frac{1}{2}\frac{\partial u^2}{\partial x} = 0.$$

- WADG yields high order convergence, correct shock speed for both $w(x)$ smooth, discontinuous (within an element).

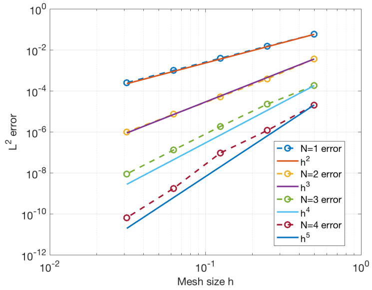


(a) Smooth solution

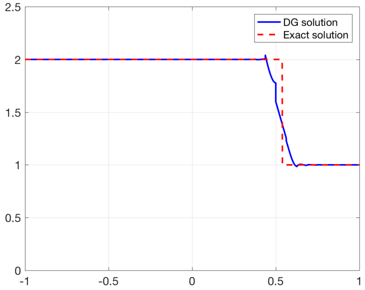


(b) Shock solution

# Effect of conservation on shock speeds

- Weighted Burgers' equation, $w(x)$ curves characteristic lines.

$$w(x)\frac{\partial u}{\partial t} + \frac{1}{2}\frac{\partial u^2}{\partial x} = 0.$$

- WADG yields high order convergence, correct shock speed for both $w(x)$ smooth, discontinuous (within an element).

Best guess: where and what is locally conserved matters;
non-conservation of *nonlinear flux* results in incorrect shock speeds.